nature nanotechnology

SUPPLEMENTARY INFORMATION

DOI: 10.1038/NNANO.2016.170

Notch filtering the nuclear environment of a spin qubit

The supplementary information is divided into sections, which discuss the following topics:

1. Calibration of π pulses
2. Semiclassical model of decoherence due to nuclear noise
3. Estimating N and δB from Hahn echo signal
4. Estimating $T_{\rm SD}$ and β from scaling of coherence time
5. Extension of the model to take into account anisotropy of electron g-factor. Discussion of the origin of the splitting of the first revival peak.

1. Calibration of π pulses

To generate decoupling sequences consisting of as many as 1000 π pulses we took advantage of charge-noise-insensitive symmetric exchange pulses. This new technique improves the quality factor of exchange oscillations by a factor of six relative to conventional method of tilting the double dot potential [S1, S2]. A detailed analysis of this technique, and results obtained in the preceding experiment from the same setup and same sample, can be found in Ref. [S1, S3].

The optimization was performed by maximizing the Hahn echo signal by varying the amplitude of the symmetric exchange pulse, γ_X, while keeping detuning $\varepsilon_X = 0$ mV, exchange time $t_X = 4.167$ ns and total evolution time $\tau = 0.75$ μs fixed (Fig. S1). The experiment was performed on the same device and in identical tuning as Ref. [S1], where γ_X and ε_X are defined and discussed in detail.

We note that symmetric exchange pulses show a weaker dependence on gate voltages than ordinary tilt pulses. Hence, symmetric π pulses are more robust against fluctuations of pulse amplitudes. On the other hand, symmetric pulses require a larger amplitude, resulting in somewhat slower exchange gates compared to conventional tilted exchange gates. This limitation makes π pulses more susceptible to errors induced by gradients of the Overhauser field, causing a tilted rotation axis of the qubit. In future experiments, larger pulse amplitudes can be achieved straightforwardly by decreasing the attenuation in the transmission lines in the cryostat.

Nevertheless, the CPMG sequence is particularly robust to two kinds of π pulse errors that affect exchange gates [S4]. The first is over or under rotation around the vertical axis of the Bloch sphere due to miscalibration of pulse amplitude and duration. The second is tilt of the rotation axis in the $|S\rangle$-$|T_0\rangle$–$|\uparrow\downarrow\rangle$-$|\downarrow\uparrow\rangle$ plane due to uncontrolled gradients of the Overhauser field.

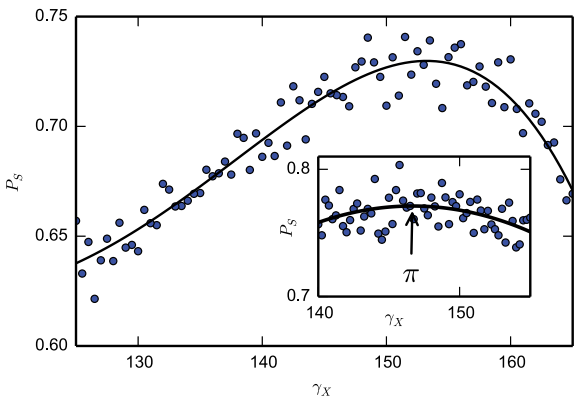

FIG. S1: **Calibration of π pulses** Singlet return probability P_S as a function of a symmetric exchange pulse amplitude, for exchange time of 4.167 ns in a Hahn echo experiment. The maximum probability indicates π pulse. Solid line is a guide to the eye. Inset: around the maximum the parabola is fitted to the data. Symbol π indicates value of γ_X corresponding to the π pulse.

2. Semiclassical model for decoherence

The inset of Fig. 4 shows theoretical results for coherence revivals. The model is derived closely following the semiclassical approach developed in Ref. [S5]. The starting point is to express the Hamiltonian for the $|\uparrow\downarrow\rangle$, $|\downarrow\uparrow\rangle$ subspace of the two-spin system as

$$\hat{H}(t) = g^* \mu_B \sum_{d=L,R} \left(B^{\rm nuc}_{z,d}(t) + \frac{|\mathbf{B}^{\rm nuc}_{\perp,d}(t)|^2}{2|\mathbf{B}^{\rm ext}|} \right) c(t) \hat{S}^z_d, \tag{S1}$$

where g^* is the electron g-factor, μ_B is the Bohr magneton, $\mathbf{B}^{\rm ext}$ is the external magnetic field, $B^{\rm nuc}_{z,d}$ ($\mathbf{B}^{\rm nuc}_{\perp,d}$) is the Overhauser field component parallel (perpendicular) to external magnetic field, $\hat{S}^z_d$ is the electron spin operator, $d = L, R$ labels the left and right dots, and we assume $|\mathbf{B}^{\rm ext}| \gg |\mathbf{B}^{\rm nuc}_d|$. Here, the sequence of π pulses

DOI: 10.1038/NNANO.2016.170

applied to the qubit is captured by

$$c(t) = \sum_{j=0}^{n} (-1)^j \theta(t_{j+1} - t)\theta(t - t_j), \qquad \text{(S2)}$$

where t_j is the time at which the j-th π pulse of the CPMG sequence is applied (with $t_0 = 0$, $t_{n+1} = T$), and $\theta(t)$ is the Heaviside step function.

Reference [S5] treated only the Hahn echo sequence. This corresponds to $n = 1$ in the above. Following the same sequence of steps, we obtain results for arbitrary n. As in that case, the decoherence function $W(\tau) = W_z(\tau)W_\perp(\tau)$ is separated into a product of contributions from the longitudinal and transverse noise sources. The low-frequency longitudinal noise contribution is of the form $W_z(\tau) = e^{-(\tau/T_{\rm SD})^\alpha}$, where $\alpha = \beta + 1$ is related to the exponent in the power law $1/f^\beta$ describing the spectrum of this noise source [S6], and $T_{\rm SD}$ is the spectral diffusion time. Because the transverse field enters the Hamiltonian (S1) as a square, $|\mathbf{B}^{\rm nuc}_{\perp,d}(t)|^2$, this noise source is effectively non-Gaussian [S5, S7]. As a result, the decoherence function for dot d is of the form $W_{\perp,d}(\tau) = 1/\det(1+iT_d)$ with components of the matrix T_d given by

$$T_{kl,d} = \frac{5A_{\xi(k)}A_{\xi(l)}\sqrt{N_k N_l}}{2g^*\mu_B|\mathbf{B}^{\rm ext}|}\frac{\omega_{kl}}{\omega_{kl}^2 - A_{kl}^2}\left\{1 - \frac{\cos\left(\frac{A_{kl}T}{2n}\right)}{\cos\left(\frac{\omega_{kl}T}{2n}\right)}\right\}\sin\left(\frac{\omega_{kl}T + n\pi}{2}\right)e^{i\frac{\omega_{kl}T+n\pi}{2}}. \qquad \text{(S3)}$$

Here k, l labels groups of nuclei associated by isotope and local nuclear Zeeman coupling, $A_{\xi(k)}$ is the hyperfine coupling constant for nuclei in group k, $A_{kl} = A_{\xi(k)} - A_{\xi(l)}$, N_k is number of nuclei in a group, $\omega_{kl} = \omega_k - \omega_l$ is a difference of Larmor frequencies between nuclei from two groups, and $T = n\tau$ is the total evolution time. Specifically, the nuclei of each isotope are divided into K groups using the relation $N_k = n_{\xi(k)}N/(2K)$, where n_ξ is the number of nuclei of isotope ξ per unit cell, and where all nuclei within each group have the same Larmor angular frequency ω_k. The value of ω_k for each group is drawn from a Gaussian distribution centered at the bare Larmor frequency ω_ξ for the corresponding isotope, with standard deviation δB. The broadening δB is introduced as a phenomenological parameter to take into account an effective spread in the Larmor frequencies due to inhomogeneous quadrupolar splittings and dipole-dipole interactions. For the simulation shown in Fig. 4, differences between hyperfine couplings within the same isotope were neglected, and convergence was obtained with $K = 4$ groups.

Larmor frequencies and hyperfine couplings used to perform the simulation shown in Fig. 4 were taken from Ref. [S8] (table S1). The remaining parameters are: the effective number, N, of nuclei interacting with each electron, inhomogeneity, δB, of the effective magnetic field acting on the nuclei, the spectral diffusion time, $T_{\rm SD}$, and the exponent, β, associated with the low-frequency noise. The following sections explain how these parameters are obtained.

3. Estimating N and δB from Hahn echo signal

The simulation of revivals under CPMG sequences requires knowledge of four device-specific parameters, two of which, the effective number, N, of nuclei interacting with each electron and the inhomogeneity, δB, of the effective magnetic field acting on the nuclei, are extracted from Hahn echo data obtained at several magnetic fields (Fig. S2). Following previous work [S5, S9] we first fit theory to Hahn echo data at each magnetic field separately, keeping δB, N, the spectral diffusion time for Hahn echo, $T_{\rm SD}^{\rm Hahn}$, vertical offset, and vertical scaling as free parameters. Setting $T_{\rm SD}^{\rm Hahn} \gg 1$ ms gives essentially equally good fits (i.e. $T_{\rm SD}^{\rm Hahn}$ cannot be determined accurately by this method) but values for δB and N obtained at various magnetic fields (150-350 mT) differ from each other by less than 20%. Therefore we average these values and obtain $\delta B = 1.1$ mT and $N = 7 \times 10^5$. Fixing these values and $T_{\rm SD}^{\rm Hahn} = \infty$, we leave the vertical offset and vertical scaling as the only free parameters, and obtain excellent agreement for all magnetic fields, as seen in Fig. S2. Visibility and offset are left as free parameters, independent for each curve, to accommodate a fluctuating readout visibility that is likely due to a buildup of the gradient of Overhauser field for large $B^{\rm ext}$ [S10].

TABLE S1: Bare Larmor angular frequencies, ω_ξ, hyperfine constants, A_ξ, in units of angular frequency, and abundances, n_ξ, of ^{69}Ga, ^{71}Ga and ^{75}As, taken from Ref. [S8].

	ω_ξ/B [s^{-1}T^{-1}]	A_ξ [s^{-1}]	n_ξ
^{69}Ga	64.2	5.47×10^{10}	0.604
^{71}Ga	81.6	6.99×10^{10}	0.396
^{75}As	45.8	6.53×10^{10}	1

The only systematic deviation between the experimental results and the model is a slight, rapid, initial decay of the signal (first 3-5 data points of each data set). This effect was also observed in Refs. [S9, S11]. The effect depended on the external magnetic field as well as the gradient of the Overhauser field [S11], and was speculated to be related to the entanglement of the qubit with the nuclear bath or to π pulse errors [S9].

4. Estimating T_{SD} and β scaling of coherence time

To estimate the spectral diffusion time T_{SD} for the simulation in Fig. 4a we quantify the scaling of the CPMG coherence time with the number of π pulses n in a regime where revivals are not yet developed (i.e., for $n \leq 32$ at 750 mT) [S6]. The coherence time is found to be proportional to n^{γ}, with $\gamma \sim 0.75$ [S12]. Using this scaling behaviour we infer $T_{\mathrm{SD}} \approx 0.6$ ms for a CPMG sequence with 256 π-pulses. Using the relationship $\beta = \gamma/(1-\gamma)$ [S6] the exponent $\gamma = 0.75$ corresponds to a power law of low-frequency noise governed by $1/f^{\beta}$ behaviour, with $\beta = 3$, in reasonable agreement with previous measurements [S6].

5. Splitting of the first revival peak

A possible explanation for the observed splitting in the first revival peak (Fig. 4a) is based on the anisotropy of the electronic g-factor. The g-factor anisotropy between [011] and [01-1] primary axes can be as high as 15% in asymmetric GaAs/AlGaAs quantum wells [S13]. In Ref. [S11] it was shown that the anisotropy has a strong impact on S-T_0 qubit coherence when the magnetic field is not parallel to one of the main axes. The combination of the anisotropy and small misalignment of the external magnetic field with the [011] crystal axis changes the magnetic field term in the system Hamiltonian (S1) to:

$$B^{\mathrm{nuc}}_{z,d}(t) + \frac{|\mathbf{B}^{\mathrm{nuc}}_{\perp,d}(t)|^2}{2|\mathbf{B}^{\mathrm{ext}}|} + \frac{g_{\perp}}{g_{\parallel}}\left[B^{\mathrm{nuc}}_{x,d}(t) + B^{\mathrm{nuc}}_{y,d}(t)\right], \quad \text{(S4)}$$

where $g_{\parallel}$ ($g_{\perp}$) are diagonal (off-diagonal) elements of a g-tensor in the basis set by direction of the external magnetic field. The latter leads to the appearance of individual nuclear Larmor frequencies in the nuclear noise spectrum in addition to nuclear difference frequencies [S11]. As a result, the CPMG sequence will not be as efficient in suppressing nuclear noise even when the pulses are commensurate with all three difference frequencies.

In Fig. S3 we present simulations showing the consequences of g-factor anisotropy. Panel (a) shows the simulation presented in the inset of Fig. 4a, i.e. $g_{\perp}/g_{\parallel} = 0$. In panel (b) we show a simulation that assumes $g_{\perp}/g_{\parallel} = 0.01$. Although our external magnetic field was nominally aligned with the [011] crystal axis (cf. Fig. 1a), the choice of $g_{\perp}/g_{\parallel} = 0.01$ is consistent with the smallest value observed in [S11] for the same direction of magnetic field as in our setup. In our simulation a splitting of the first revival peak appears (indicated by a white arrow) as well as more complex fine structure in other revival peaks. Such fine structure is beyond the resolution of the experimental data.

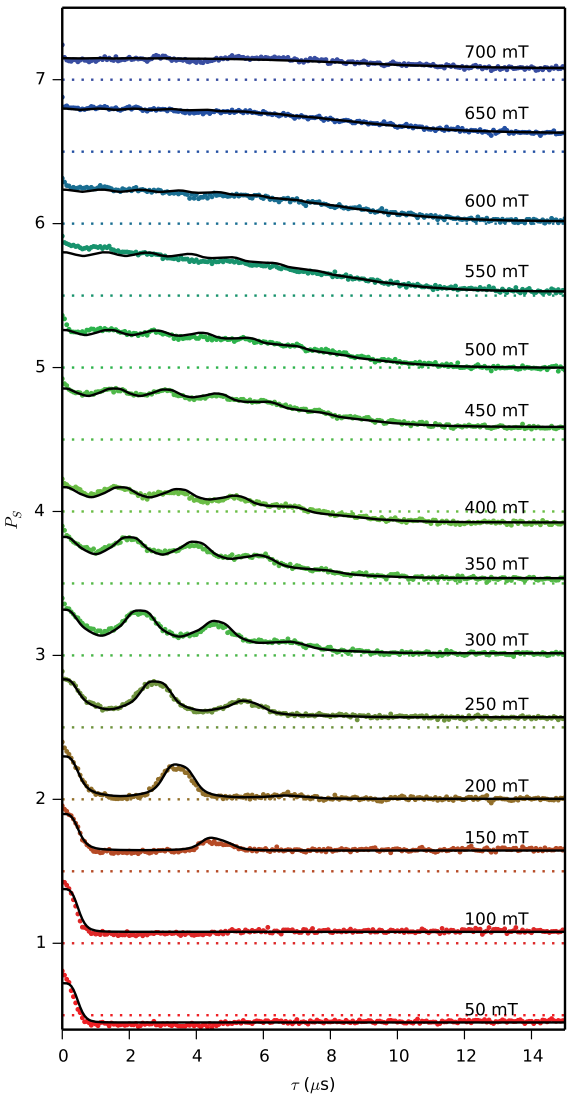

FIG. S2: **Revival of coherence under Hahn-echo sequence.** Singlet return probability P_S as a function of separation time τ for various magnetic fields. Datasets are offset for clarity. Dotted lines indicate $P_S = 0.5$ for data plotted in corresponding color. Black lines are simulations with $\delta B = 1.1$ mT, $T_{\mathrm{SD}}^{\mathrm{Hahn}} = \infty$, $N = 7 \times 10^5$. They are fitted to experimental data using offset and visibility, different for each curve.

DOI: 10.1038/NNANO.2016.170

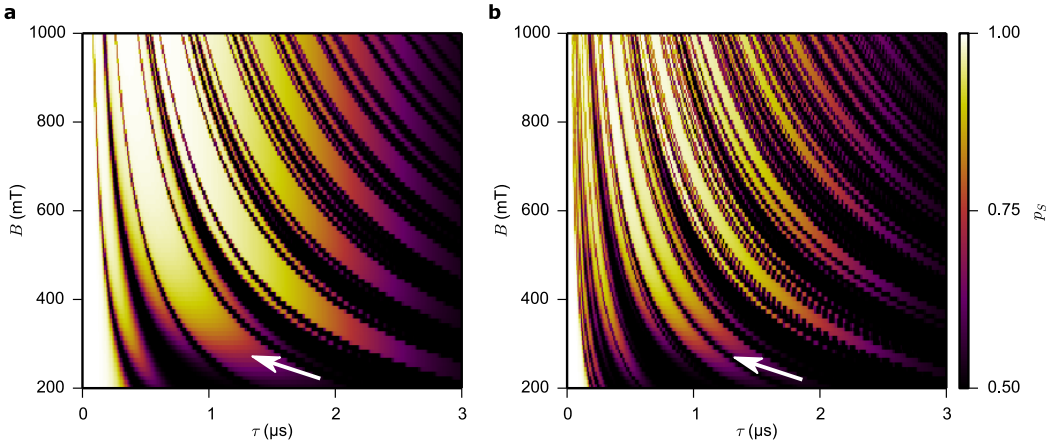

FIG. S3: **Simulation of revivals of coherence under CPMG sequence for 256 π pulses. a**, Simulation omitting effects of g-factor anisotropy, identical to map in the inset of Fig. 4a, i.e., $g_\perp/g_\parallel = 0$. **b**, Simulation assuming $g_\perp/g_\parallel = 0.01$.

We note that a splitting of the first revival peak appears exactly when the frequency of π pulses coincides with a difference of Larmor frequencies $f_{^{71}\mathrm{Ga}} - f_{^{69}\mathrm{Ga}}$ and $f_{^{69}\mathrm{Ga}} - f_{^{75}\mathrm{As}}$. Therefore other mechanisms might also lead to the appearance of the splitting. We speculate that weak driving of the nuclei by a periodic Knight field could enhance flip-flops between nuclei of different species and therefore increase spin diffusion, leading to faster decoherence.

[S1] Martins, F. *et al.* Noise suppression using symmetric exchange gates in spin qubits. *Phys. Rev. Lett.* **116**, 116801 (2016).

[S2] Reed, M. *et al.* Reduced Sensitivity to Charge Noise in Semiconductor Spin Qubits via Symmetric Operation. *Phys. Rev. Lett.* **116**, 110402 (2016).

[S3] Barnes, E. *et al.* Filter function formalism beyond pure dephasing and non-Markovian noise in singlet-triplet qubits. *Phys. Rev. B* **93**, 121407 (2016).

[S4] Borneman, T. W., Hürlimann, M. D. & Cory, D. G. Application of optimal control to CPMG refocusing pulse design. *J. Magn. Reson.* **207**, 220–233 (2010).

[S5] Neder, I. *et al.* Semiclassical model for the dephasing of a two-electron spin qubit coupled to a coherently evolving nuclear spin bath. *Phys. Rev. B* **84**, 035441 (2011).

[S6] Medford, J. *et al.* Scaling of Dynamical Decoupling for Spin Qubits. *Phys. Rev. Lett.* **108**, 086802 (2012).

[S7] Cywiński, Ł. Dynamical-decoupling noise spectroscopy at an optimal working point of a qubit. *Phys. Rev. A* **90**, 042307 (2014).

[S8] Cywiński, Ł., Witzel, W. M. & Das Sarma, S. Pure quantum dephasing of a solid-state electron spin qubit in a large nuclear spin bath coupled by long-range hyperfine-mediated interactions. *Phys. Rev. B* **79**, 245314 (2009).

[S9] Bluhm, H. *et al.* Dephasing time of GaAs electron-spin qubits coupled to a nuclear bath exceeding 200μs. *Nat. Phys.* **7**, 109–113 (2011).

[S10] Barthel, C. *et al.* Relaxation and readout visibility of a singlet-triplet qubit in an Overhauser field gradient. *Phys. Rev. B* **85**, 035306 (2012).

[S11] Botzem, T. *et al.* Quadrupolar and anisotropy effects on dephasing in two-electron spin qubits in GaAs. *Nat. Commun.* **7**, 11170 (2016).

[S12] Malinowski, F. K., Martins, F., Nissen, P. D., Cywiński, Ł., Rudner, M. S., Fallahi, S., Gardner, G. C., Manfra, M. J., Marcus, C. M. & Kuemmeth, F. (in preparation).

[S13] Nefyodov, Y. A., Shchepetilnikov, A. V., Kukushkin, I. V., Dietsche, W. & Schmult, S. Electron g-factor anisotropy in GaAs/$Al_{1-x}Ga_xAs$ quantum wells of different symmetry. *Phys. Rev. B* **84**, 233302 (2011).